Composites: Part B 50 (2013) 247–252

Contents lists available at SciVerse ScienceDirect

Composites: Part B

journal homepage: www.elsevier.com/locate/compositesb

Modelling of adhesive bonding for aircraft structures applying the insertion squeeze flow method

P. Burka [a,*], X. Liu [b], M.C. Thompson [a], J. Sheridan [a]

[a] Fluids Laboratory for Aeronautical and Industrial Engineering (FLAIR), Department of Mechanical & Aerospace Engineering, Monash University, 4100 Victoria, Australia
[b] Cooperative Research Centre for Advanced Composite Structures Ltd., 506 Lorimer Street, Fishermans Bend, 3207 Victoria, Australia

ARTICLE INFO

Article history:
Received 7 November 2012
Received in revised form 2 February 2013
Accepted 20 February 2013
Available online 27 February 2013

Keywords:
A. Carbon fibre
B. Rheological properties
C. Computational modelling
E. Joints/joining

ABSTRACT

A numerical model for simulating the flow of an adhesive during an insertion squeeze flow (ISF) bonding process for joining composite structures is presented. The model is developed using the commercial CFD code FLUENT®. The numerical model is validated for a Newtonian fluid by comparing the predicted insertion forces that act during the insertion process with those obtained both from experiments and calculated using a simplified analytical model. Very good agreement is obtained. The model is then used to investigate the effect of insertion speed and adhesive viscosity on the ISF bonding process. The findings, and the further application of the numerical and analytical models, are valuable to ensure the quality of Pi-slot joints.

1. Introduction

The process of adhesive bonding of composite components for aircraft manufacture is not only a fibre-friendly joining method, but it also provides significant weight and cost savings potential compared to the use of mechanical fasteners [1,2]. Matthews [3] elaborates further on the advantages, in particular, less stress concentration around the holes that are provided for fasteners, and emphasises that during adhesive bonding fibres are not damaged through the process of hole drilling as they are when mechanical fasteners are used. Several studies on adhesive bonding of composite spar to skin applications have been conducted before. A relatively early example where a Pi(π)-shaped joint design was applied for adhesive bonding of aircraft structures can be found in Wong [4]. Wong [4] presents the development of sandwich constructions for an all composite aircraft. Of specific relevance for the presented work is the main wing consisting of a top and bottom sandwich skin, with the bottom skin having an integrated stiffener. Bonding is realised by utilising a cure paste adhesive. Ritter [1] and Russel [5] emphasise the cost and weight-saving potential of adhesive bonding for composite components. Russel [5] further summarizes the contents and achievements of the Composite Affordability Initiative (CAI), a program investigating the application of adhesive bonding for composite aircraft structures. The selected joint design was the Pi(π)-joint with the roof of the Pi(π) being co-bonded or co-cured to the skin. The adhesive distribution is said to be regarded as challenging and critical, as in similar joint-structures out-times are experienced and adhesive exposure to air is observed. However, neither Wong [4] nor Russel [5] provide insight or details on the dynamics and kinematics of the insertion process.

The present paper describes a numerical solution that models the insertion squeeze flow (ISF) taking place during the adhesive bonding of modular Pi(π)-shaped composite joints. Using the general purpose computational fluid dynamics (CFD) code FLUENT®, a model was developed for Newtonian fluids initially. The numerical solution was verified against an analytical solution that was derived for the flow problem investigated. Good agreement was obtained, indicating the developed numerical solution provides meaningful results and hence provides confidence that the numerical model could be further modified to simulate the flow of non-Newtonian fluids.

Five parameter rational models were found to well represent the non-Newtonian, shear-thinning behaviour of the adhesives used. After implementing the non-Newtonian stress strain-rate rheological models into the overall numerical model, simulations were conducted to study the effect of insertion speed and adhesive viscosity on insertion forces.

2. Development of the numerical model

2.1. Model description

Fig. 1 shows a typical example of a type of joint considered for the current research. It is composed of an insertion plate and a

* Corresponding author. Tel.: +49 1577 3343721.
E-mail address: pat_burka@gmx.net (P. Burka).

1359-8368/$ - see front matter © 2013 Elsevier Ltd. All rights reserved.
http://dx.doi.org/10.1016/j.compositesb.2013.02.019

Pi-slot for the simulation of adhesive flow during ISF. For typical aircraft applications, the joints required are often relatively long—typically more than 1000 mm in length—and the adhesive needs pre-applied into the Pi-slot relatively uniformly along the length. For the purposes of the numerical model, it is assumed that the adhesive flow can be simplified as a two-dimensional (2D) flow through a cross-section of the joint. Initially the adhesive is contained at the bottom of the Pi-slot below the insertion plate starting position. When the insertion plate moves downwards, the adhesive is forced to flow upwards into the narrow channels between the insertion plate and Pi-slot walls. The key dimensions defining the geometry are: height of the Pi-slot, H_1, initial height of the adhesive, H_0, and widths of the insertion plate and Pi-slot, $2a$ and $2b$, respectively. The flow channel width δ results from the width of the insertion plate and Pi-slot, and is simply $b–a$ in the case when the insertion plate is perfectly centred between the Pi-slot walls. The length (into the page) is L.

The numerical work conducted was performed using the commercial computational fluid dynamics software package ANSYS® FLUENT® 6. Fluent 6 utilises a finite-volume approach to numerically solve the Navier–Stokes equations. To model the fluid–fluid interface (air and adhesive), the volume-of-fluid (VOF) incorporated in Fluent 6 was applied. An important assumption of the VOF method, which is reasonable in this case, is that the fluids do not interpenetrate [6]. A dynamic mesh model available in Fluent 6 enables simulations where the domain changes with time due to motion of domain boundaries. Hence, a moving boundary script was developed and implemented so that a prescribed translational motion could be applied to the insertion plate walls. All other walls were specified as solid wall entities, which were rigid and impermeable with a no-slip boundary condition applied. The flow domain was then defined as the space between these walls.The full mesh set-up as well as details of the set-up are presented in Figs. 2 and 3.

The fluids within the domain were modelled as two phases: air and adhesive. Initially, to simplify the problem and allow validation, the adhesive was modelled as a Newtonian fluid. Subsequently the adhesive model was changed to a five-parameter rational model, which relates the adhesive shear viscosity and the shear rate accurately over the entire shear rate range. In this way the effect of the shear thinning nature of the adhesive on output parameters could be predicted. As an example of the numerical results Fig. 4 illustrates the distribution of the adhesive and air within the flow channels.

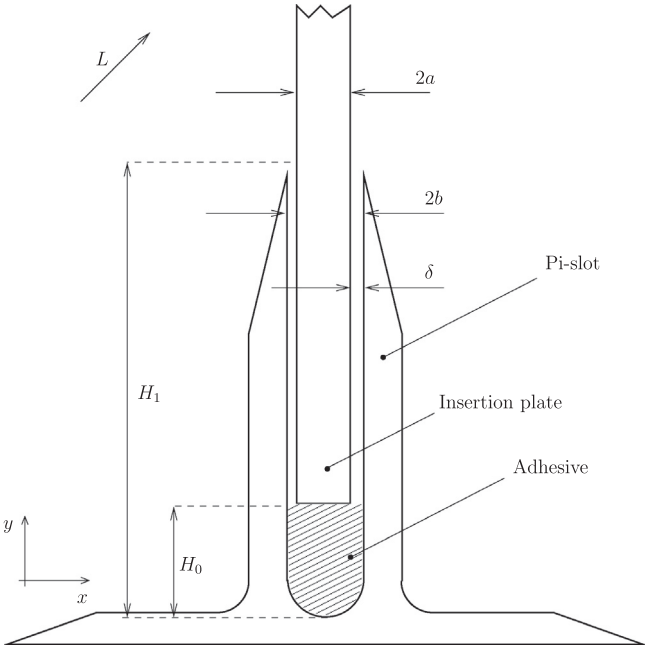

Fig. 1. Key dimensions for 2D simulation of Pi-slot joint.

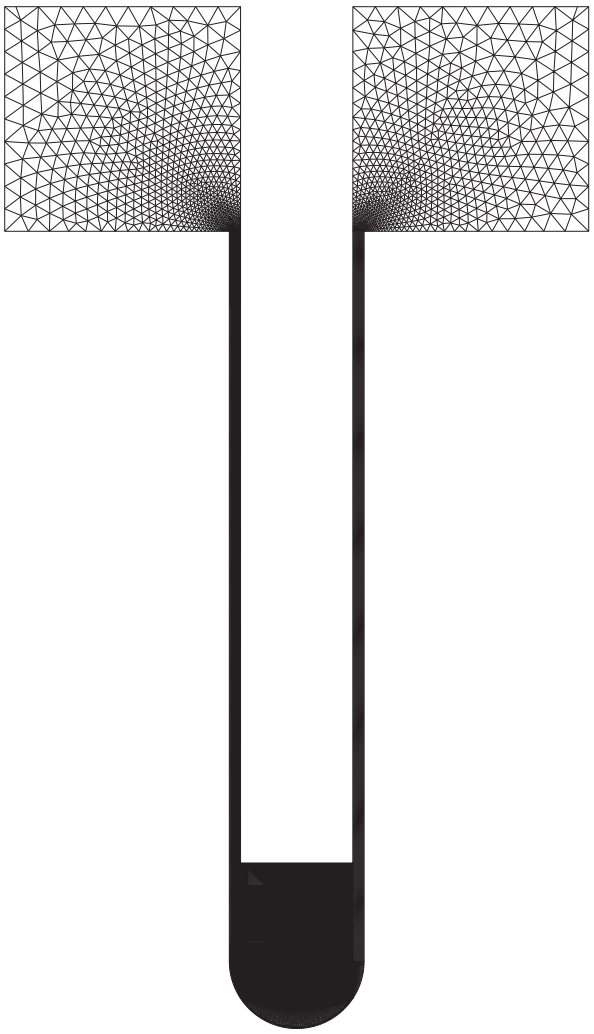

Fig. 2. Full mesh set-up for modelling of the insertion squeeze flow for adhesive bonding of composite structures.

2.2. Development of the analytic model

An analytical model is derived based on a procedure applied for a similar problem proposed by Smith et al. [7] and considers the flow of Newtonian fluids only. We developed a model that allows the calculation of insertion forces and velocity distributions within the flow channels for the considered geometry. The analytical model assumes one-dimensional flow in the channels, which presumably should be a good approximation away from the adhesive reservoir at the bottom. The remaining terms in the incompressible Navier–Stokes equations are those representing a balance between pressure and viscous forces:

$$\frac{dp}{dy} + \mu \frac{d^2 v}{dx^2} = 0, \tag{1}$$

where p is pressure, v is vertical velocity and μ is the molecular viscosity. Explicitly, the derivation is based on two assumptions: the pressure p and velocity v are functions of y and x, respectively, only. Integrating this equation with regard to x and solving for the integration constants using the no-slip boundary conditions at $x = a$

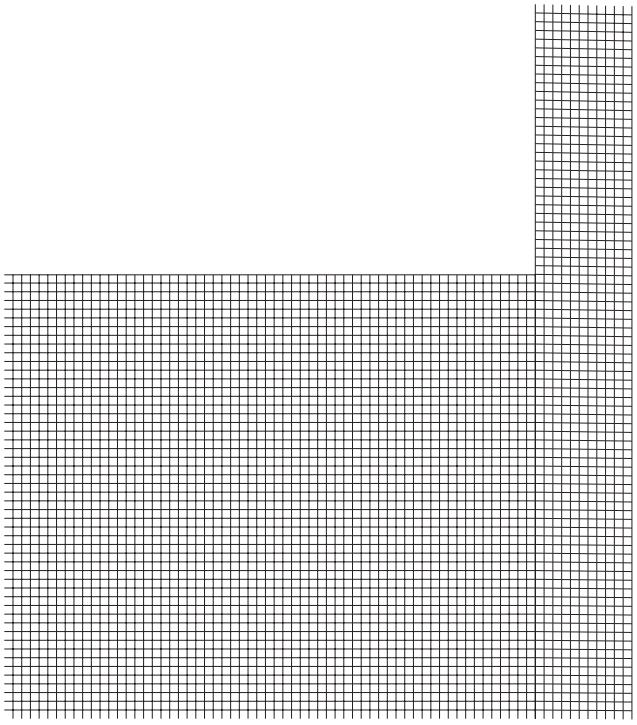

Fig. 3. Mesh detail for modelling of the insertion squeeze flow for adhesive bonding of composite structures.

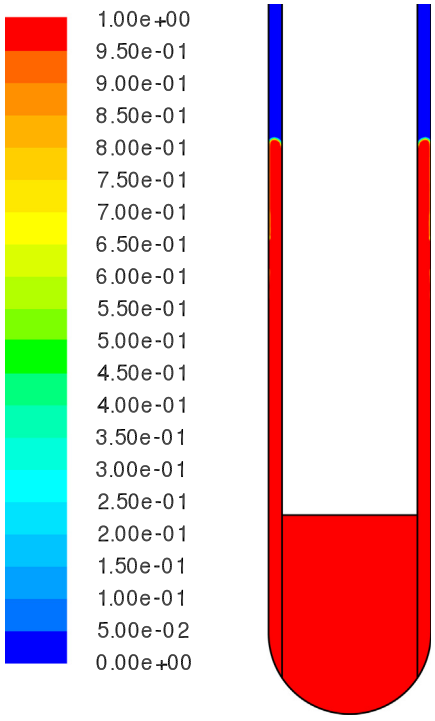

Fig. 4. Numerical result showing the flow of adhesive and air within the flow channels during the insertion squeeze flow bonding process.

and $x = b$, gives the following expression for the velocity distribution as a function of distance across the gap (x)

$$v(x) = \frac{1}{\mu}\frac{dp}{dy}\frac{x^2}{2} + \left(-\frac{V}{a-b} - \frac{1}{\mu}\frac{dp}{dy}\frac{a+b}{2}\right)x + V\frac{b}{a-b} + \frac{1}{\mu}\frac{dp}{dy} \times \frac{ab}{2}. \quad (2)$$

The insertion force consists of two components [7], namely the pressure force due to pressure built up at the bottom of the moving insertion plate and a viscous drag force at the contact surface between the insertion plate and the fluid. This allows the insertion force per unit width (F/L) to be expressed as

$$\frac{F}{L} = -2\mu c V\left[3\frac{(a+b)^2}{(a-b)^3} + \frac{1}{a-b}\right]. \quad (3)$$

Here L is the Pi-joint length into the page, c is the flow front height of the adhesive within the flow channel and V is the insertion speed. The above equation indicates that for a Newtonian fluid, the insertion force increases linearly with viscosity, insertion speed and flow front height.

Insertion forces calculated applying Eq. (3) were compared with numerical predictions of the insertion forces for different insertion speeds (top of Fig. 5) and different adhesive viscosities (bottom of Fig. 5). For a variation of the insertion speed between 2 and 10 mm/min (top figure), the adhesive viscosity was set 1000 Pa s. When varying the adhesive viscosity (500, 1000, 2000 Pa s, bottom figure), the insertion speed was fixed at 5 mm/min.

Fig. 5 indicates for both cases that the insertion force increases linearly with respect to time over the time range considered. Further, the insertion force also increases linearly with respect to insertion speed (top of Fig. 5). For example, increasing the insertion force by a factor of two (5–10 mm/min) leads to an approximately doubling of the insertion force (at $t^* = 1$, the numerical predictions were 4842 N/m and 9782 N/m, respectively, i.e., the higher insertion force is double the lower one to within 2%). Note that the non-dimensional time, t^*, is time divided by the time required for the adhesive to reach the top of the Pi-slot.

Considering the effect of the viscosity on the insertion force, it is observed that the insertion force again increases linearly with respect to viscosity and time.

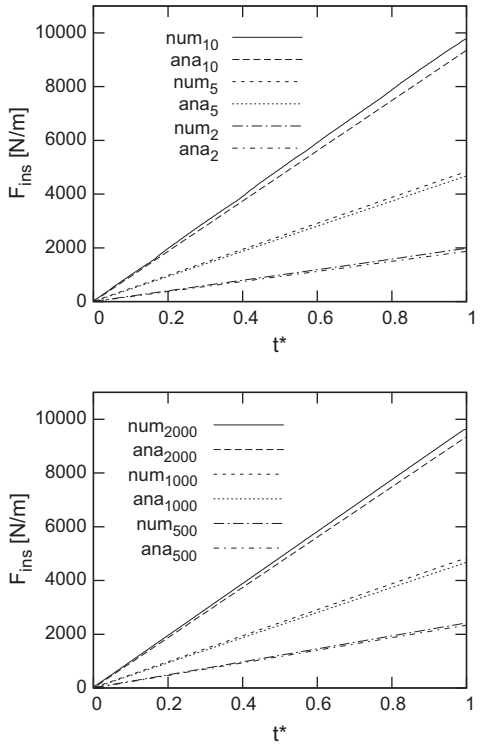

Fig. 5. Insertion force per unit width F_{ins} against non-dimensional time t^*. Top figure: Adhesive viscosity was set to 1000 Pa s, with insertion speed varied. Bottom figure: insertion speed set to 5 mm/s, with viscosity varied.

In general, good agreement between the analytical and the numerical models was obtained. The discrepancy was between 4.0% and 5.6% for a variation of the insertion speed, and between 3.6% and 4.0% for a variation of the adhesive viscosity. The numerical model consistently predicted higher insertion forces. The differences observed between the insertion force predictions are caused by simplifications in the analytical model. The main source of error is due to the assumption of one-dimensional flow and pressure variation, which break down slightly at the bottom of the Pi-slot.

2.3. Constitutive models for non-Newtonian adhesives

The epoxy adhesives used for the study consisted of different combinations of two commercially available adhesives EA 9395 and EA 9396. The latter has a lower viscosity, hence adjusting the combination allows the viscosity to be varied. For the current research the stress strain-rate relationship was determined using a Rheometrics Fluid Spectrometer II (RFS II) (Rheometrics Inc., New Jersey, USA). Three different mixture ratios were used for the experiments consisting of 100:0%, 85:15% and 70:30% by weight mixtures of EA 9395 and EA 9396. Each rheometric test was conducted four times with the average result used to characteristise the behaviour. Each of the epoxy mixtures showed clear non-Newtonian shear-thinning behaviour. Thixotropic loop tests were conducted, which revealed only relatively minor hysteretic variation, thus it appeared reasonable to neglect time-dependent history effects at least for the development of the initial model. Dynamic oscillation tests were also performed to investigate viscoelasticity. From determined relaxation times, the Deborah number (De), which relates the relaxation time to the process time [8], was derived, and was found to be $De \ll 1$. Elasticity effects can be assumed to be negligible under this condition (e.g., [9]). Hence, given that time-dependence and elasticity effects could be ignored, the model development focussed only on the shear viscosity versus shear-rate dependence. In Fig. 6, the adhesive shear viscosity is plotted with respect to shear rate for the 70:30 mixture. A five parameter rational fit is illustrated.

The shear viscosities calculated from the model agree very well with the measurements over the whole shear rate range considered. The equation describing the five parameter rational model is

$$\mu = \frac{c_1 + c_2\frac{d\gamma}{dt} + c_3\frac{d\gamma}{dt}^2}{1 + c_4\frac{d\gamma}{dt} + c_5\frac{d\gamma}{dt}^2}, \tag{4}$$

with c_1, c_2, c_3, c_4 and c_5 being the fitting constants. In order to cover the typical viscosity range used in practice, as indicated above, three different adhesive combinations were used for the experiments and numerical simulations. The lower viscosity limit acceptable is the one for a weight ratio of 70:30% EA 9395 to EA 9396. The most viscous adhesive considered in this research consisted of EA 9395 only. In each case, the five parameter rational model fit was obtained, and in each case the model fit agreed very well with the raw data. Consequently, this rheological model was used for each mixture to represent the shear-thinning behaviour in the overall numerical model.

The fitting parameters for the three adhesive mixtures, representative of typical high, intermediate and low viscosity adhesives, are given in Table 1.

Table 1
Fitting constants for the five-parameter shear-thinning model for different mixture ratios.

wt.% EA 9395:EA 9396	c_1	c_2	c_3	c_4	c_5
100:0	16024.99	13515.67	1080.79	83.276	23.120
85:15	5293.645	6541.795	891.0529	66.909	36.160
70:30	1738.666	2216.062	318.678	38.981	13.796

3. ISF at constant insertion speed

3.1. Effect of insertion speed

As described in Section 2.1, the ISF process was modelled two-dimensionally on a cross section through the joint. A constant speed condition was applied on the wall boundaries that represent the insertion plate walls. Because of this motion the adhesive was displaced into the flow channels that form between the insertion plate side walls and the Pi-slot wall boundaries. The input parameters that were varied were the insertion speed and the adhesive viscosity. The insertion speeds investigated were 2.5, 5 and 10 mm/min. Both flow channel widths were fixed during the insertion process at $\delta = 0.5$ mm, with $a = 3$ mm and $b = 2.5$ mm. The Pi-slot height H_1 was 35.5 mm. The material properties of air were density $\rho = 1.2$ kg m^{-3} and molecular viscosity $\mu = 0.00002$ kg m^{-1} s^{-1}. The initial adhesive amount was 105 vol.% of the amount necessary to fill the flow channels completely at the final insertion position. The initial adhesive height H_0 could be derived from this amount. The effect of insertion speed on the insertion force with respect to dimensionless time is presented in Fig. 7 for the 70:30 mixture.

As discussed for the Newtonian model, the insertion force presented in Fig. 7 consists of two components, the pressure force that acts perpendicular to the insertion plate head and the shear force acting along the side walls of the insertion plate. The insertion force acts in the y-direction due to the resistance of the adhesive movement. For t^* greater than one, the adhesive flows out of the top of the flow channel.

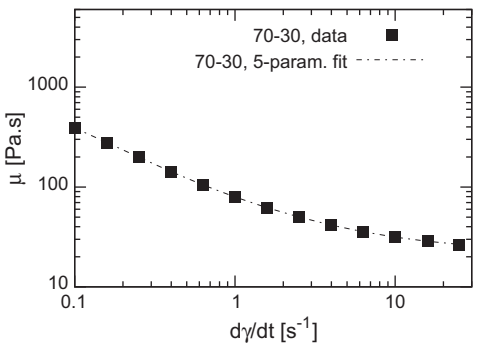

Fig. 6. Measured shear viscosity against shear-rate and five parameter rational fit for the 70:30 wt.% ratio mixture.

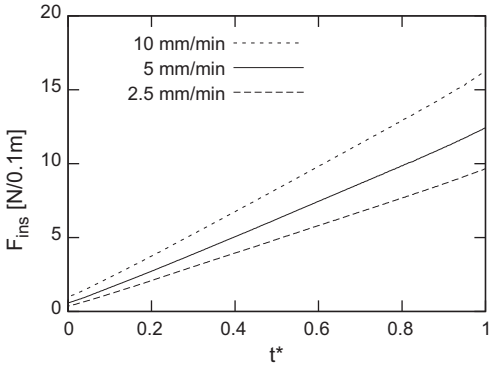

Fig. 7. Numerically predicted F_{ins} versus t^* for various insertion speeds.

From Fig. 7, it can be seen that the insertion force still increases almost linearly with respect to dimensionless time. Also, but not surprisingly, for the same insertion position it is observed that with increasing insertion speed the insertion force also increases. However, in this case, the functional dependence is not proportional as it was for a Newtonian fluid. At a dimensionless time of $t^* = 1$, the insertion force is 9.8 N/m for an insertion speed of 2.5 mm/min. Doubling the insertion speed results in an insertion force of 12.5 N/m and a further increase of the insertion speed by a factor of two leads to an insertion force of 15.9 N/m. This is about 20% lower than direct proportionality would give. This difference is due to the shear-thinning character of non-Newtonian epoxy adhesive. Indeed Fig. 6 shows that the effective viscosity varies by approximately a factor of 10 as the shear-rate is varied over two orders of magnitude between 0.1 and 10 s^{-1}, so this observed variation in insertion force is not surprising.

3.2. Effect of adhesive viscosity

As stated in Section 2.3, the adhesive viscosity could be varied by adding the lower viscosity adhesive EA 9396 to the more viscous EA 9395. By examining various mixture ratios, the effect on viscosity on the transient insertion force was investigated numerically. The simulations were conducted at constant insertion speed (v_{ins} = 5 mm/min), the insertion plate was again centred between the Pi-slot walls and the initial adhesive amount was the same as for the previous study (105%). Adhesive viscosity effects on the insertion forces with respect to dimensionless time are illustrated in Fig. 8.

The solid line represents the transient insertion force for the pure EA 9395 adhesive. The other curves show the considerable reduction in insertion force obtained from diluting this compound with the less viscous component. The addition of 15 wt.% of the lower viscous EA 9396 to the more viscous EA 9395 decreases the insertion force by more than 50%. For comparison the insertion force at a dimensionless time of $t^* = 1$ for EA 9395 is 38.9 N/m. The insertion force at the same time decreases to 16.1 N/m after addition of the first 15 wt.% EA 9396 (a decrease of 58.6%). Increasing the amount of EA 9396 within the mixture to 30 wt.% results in an insertion force at $t^* = 1$ of 12.4 N/m which represents a further decrease of 23.0%.

3.3. Comparisons between experimentally measured and numerically predicted insertion forces

One objective of the present research program was to draw a comparison between the experimentally measured and the numerically predicted insertion forces. The ISF experiments were conducted at low insertion speeds, matching the above presented predictions. The tests were conducted in a 10 kN universal testing machine using specimens made of carbon epoxy composites that were 100 mm in length. In terms of the Pi-slot and the flow channel, all specimens were made to the baseline dimensions defined in Section 3.1 and Fig. 1. To ensure good alignment between the insertion plate and the Pi-slot, spacer wires were used. The wire diameter was adjusted based on the actual flow channel width, as determined by the insertion plate and Pi-slot dimensions. These can vary from the nominal values due to manufacturing tolerances. The initial adhesive amount placed into the Pi-slot before starting the insertion process was 125 vol.% of the amount necessary to fill the flow channels completely at the final bonding position. Fig. 9 shows two typical transient insertion force measurements with respect to dimensionless time.

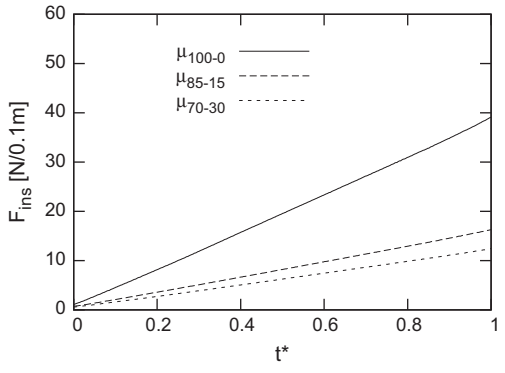

Fig. 8. F_{ins} versus t^* for various adhesive viscosities.

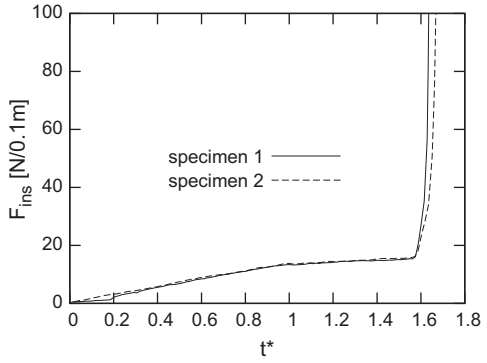

Fig. 9. Measured F_{ins} against t^* for two separate experimental test runs.

The measurements were taken at an insertion speed of 5 mm/min for the 70:30 mixture. For the first run, at the start of the insertion, a slower increase in the insertion force was recorded, resulting from the compaction of the initially uneven adhesive surface (specimen 1). For the second specimen, however, this compaction is not observed due to a more even adhesive surface. For both specimens an approximately linear increase in insertion force with time is observed until the adhesive starts to flow out of the flow channels at $t^* = 1$. The insertion force becomes approximately constant after this before increasing significantly when the insertion plate and the Pi-slot wall become very close and finally touch. The insertion forces that were used for comparison and which are presented in the following analysis were taken when the adhesive first flows out of the flow channels, i.e. at $t^* = 1$. They are referred to as *final insertion forces* in the following discussion.

In Table 2, the final insertion forces are compared for the pure EA 9395 adhesive. The input parameter varied was the insertion speed.

The table includes minimum and maximum measured final insertion forces, an average final insertion force (from either two or three experiments) and the numerically predicted forces. Also, the discrepancy between the averaged measured and the predicted forces is included. From the documented typical insertion forces it is evident that there is good agreement between the predicted and the measured values. The discrepancy is less than 3%. Also the relatively small range between the minimum and maximum measured final insertion forces reveals good repeatability of the experiments.

The effect of adhesive viscosity on the measured and the predicted final insertion forces is presented in Table 3.

Table 2
Comparison between measured and numerically predicted insertion forces: v_{ins} effect.

v_{ins}	$F_{ins,exp,min}$	$F_{ins,exp,max}$	$F_{ins,exp,\ ave}$	$F_{ins,num}$	%-Discr.
2	26.5	29.5	28.0	28.8	2.8
5	39.0	41.0	40.0	39.0	2.5
10	49.5	51.0	50.2	51.5	2.6

Table 3
Comparison between measured and numerically predicted insertion forces: μ effect.

% EA 9395:EA 9396	$F_{ins,exp,min}$	$F_{ins,exp,max}$	$F_{ins,exp,\ ave}$	$F_{ins,num}$	% Diff.
70:30	13.5	15.5	14.5	12.5	13.8
85:15	19.5	19.6	19.6	16.0	18.2
100:0	39.0	41.0	40.0	39.0	2.5

Again reasonably good agreement exists between the measured and predicted typical insertion forces for each of the adhesives considered. The final insertion forces measured experimentally are between 2.5% and 18.9% higher than the predicted ones. The likely cause of this are differences in specimen dimensions from the design values resulting from imperfect manufacturing. The widths (thicknesses) of the insertion plates which were used to investigate the effect of adhesive viscosity were found to vary between 5.08 mm and 5.20 mm, which is wider than the model insertion plate (5.00 mm). Consequently, slightly narrower flow channel widths result for the experiments, hence an increased resistance against flow of the adhesives in the flow channels exists, and consequently higher typical insertion forces are recorded [10].

In fact, the Newtonian analytical model of Eq. (3) indicates the force is dominated by the pressure term of Eq. (3) and this varies approximately as $1/\delta^3$. It is be expected that this scaling should also govern the situation for the non-Newtonian adhesive, at least approximately, so a fractional change in the gap width (i.e., $\Delta\delta/\delta$) should induce a fractional change in the force of $3\Delta\delta/\delta$. In turn, the gap width depends on the slot width and the insertion plate width. As an example, if the manufactured plate width plate width is actually $2a = 5.05$ mm, i.e., 1% larger than specified, for the nominal slot width of $2b = 6.00$ mm, this leads to the gap of $\delta = (b-a) = 0.475$ mm, rather than the nominal 0.5 mm. This is a fractional error of 5%, which would be expected to cause a 15% change in the required insertion force. In general, manufacturing errors in the slot and plate width of Δb and Δa, will cause a fractional change from the predicted force of approximately $3(\Delta b-\Delta a)/\delta$. Given that both the slot and plate widths are subject to manufacturing tolerances, the match between the experimentally determined and predicted insertion forces is extremely good. However, it does indicate that accurate insertion force predictions are quite sensitive to manufacturing tolerances; which is a point that may need to be considered during joint manufacture.

4. Conclusions

A numerical model has been developed to simulate adhesive flow in Pi-joints during a constant speed ISF bonding process. Rheological measurement reveal that the typical adhesives for bonding are primarily shear-thinning non-Newtonian fluids. The five parameter rational model is found to be a very good approximation to the effective viscosity shear-rate dependence over the relevant shear-rate range. It has been found that at constant insertion speed the insertion force increases approximately linearly with the adhesive flow front position. However, because of the shear-thinning nature of the adhesive, doubling the insertion speed does not lead to a doubling of the required insertion force. Overall the numerical prediction of the insertion forces for constant insertion speed runs was within 20% of the experimentally measured values, and usually very much less. The discrepancies appears to be mostly due to the component manufacturing tolerances, which are especially important since small variations in dimensions of the insertion plate or slot widths can result in significant changes to the gap size. The analytical solution for a Newtonian fluid indicates that the insertion force should vary approximately as the reciprocal of the gap ratio to the power of 3. This scaling is also expected to apply approximately to the non-Newtonian adhesive as well.

In general, the paper provides data that can be extrapolated for composite joints for aircraft, as well as verifying that a numerical model based on shear-thinning rheology can accurately predict the dynamical behaviour during the insertion process.

References

[1] Ritter G. Adhesive bonding studied for joints in aircraft structures. Adv Mater Processes 2005:21.
[2] MoJo. Modular joints for composite aircraft components. Appendix i. Description of work. Tech. rep.; sixth framework programme specific targeted research or innovation project MoJo; 2006.
[3] Matthews F. Joining fibre-reinforced plastics. Elsevier Science & Technology; 1987.
[4] Wong R. Sandwich constructions in the starship. In: Materials working for you in the 21st century. SAMPE symposium and exhibition, vol. 37; 1992. p. 186–97.
[5] Russel J. Composites affordability initiative: transitioning advanced aerospace technologies through cost and risk reduction. The AMMTIAC Quart 2006;1(2006).
[6] Hirt C, Nichols B. Volume of fluid (VOF) method for the dynamics of free boundaries. J Comput Phys 1981;39:201–25.
[7] Smith T, Ferry J, Schremp F. Measurements of the mechanical properties of polymer solutions by electromagnetic transducers. J Appl Phys 1948;20:144–53.
[8] Menges G, Haberstroh E, Michaeli W, Schmachtenberg E. Verhalten in der Schmelze, vol. 5. Carl Hanser Verlag Muenchen Wien; 2002.
[9] Mannan S, Whalley D, Ogunjimi Y, Williams D. Modelling of the initial stages off the anisotropic adhesive joint assembly process. In: IEEE electronic manufacturing technology symposium, Omiya, Japan; 1995. p. 142–5.
[10] Burka P. Squeeze flow during assembly of novel joints in composite aircraft components. PhD thesis, Monash University, Melbourne, Australia; 2009.